

MAGNETIC FIELD TOPOLOGY IN LOW-MASS STARS: SPECTROPOLARIMETRIC OBSERVATIONS OF M DWARFS¹

NGOC PHAN-BAO,^{2,3} JEREMY LIM,^{2,4} JEAN-FRANÇOIS DONATI,⁵ CHRISTOPHER M. JOHNS-KRULL,⁶ AND EDUARDO L. MARTÍN,^{7,8}

Draft version October 15, 2018

ABSTRACT

The magnetic field topology plays an important role in the understanding of stellar magnetic activity. While it is widely accepted that the dynamo action present in low-mass partially convective stars (e.g., the Sun) results in predominantly toroidal magnetic flux, the field topology in fully convective stars (masses below $\sim 0.35 M_{\odot}$) is still under debate. We report here our mapping of the magnetic field topology of the M4 dwarf G 164-31 (or Gl 490B), which is expected to be fully convective, based on time series data collected from 20 hours of observations spread over 3 successive nights with the ESPaDOnS spectropolarimeter. Our tomographic imaging technique applied to time series of rotationally modulated circularly polarized profiles reveals an axisymmetric large-scale poloidal magnetic field on the M4 dwarf. We then apply a synthetic spectrum fitting technique for measuring the average magnetic flux on the star. The flux measured in G 164-31 is $|Bf| = 3.2 \pm 0.4$ kG, which is significantly greater than the average value of 0.68 kG determined from the imaging technique. The difference indicates that a significant fraction of the stellar magnetic energy is stored in small-scale structures at the surface of G 164-31. Our H α emission light curve shows evidence for rotational modulation suggesting the presence of localized structure in the chromosphere of this M dwarf. The radius of the M4 dwarf derived from the rotational period and the projected equatorial velocity is at least 30% larger than that predicted from theoretical models. We argue that this discrepancy is likely primarily due to the young nature of G 164-31 rather than primarily due to magnetic field effects, indicating that age is an important factor which should be considered in the interpretation of this observational result. We also report here our polarimetric observations of five other M dwarfs with spectral types from M0 to M4.5, three of them showing strong Zeeman signatures.

Subject headings: stars: low mass — stars: magnetic fields — techniques: spectroscopic — techniques: polarimetric — stars: individual (G 164-31, Gl 890, LHS 473, KP Tau, Gl 896B, 2E 4498)

1. INTRODUCTION

Magnetic fields in the Sun and partially convective stars (e.g., G, K stars and possibly early M dwarfs) are produced by the so-called $\alpha\Omega$ dynamo mechanism operating at the interface between the convective envelope and the radiative core, where differential rotation is strongest, known as the tachocline. The action of differential rotation on a weak poloidal field at the base of the convective zone results in a large-scale and predominantly toroidal sub-surface field produced by this dy-

namo action (Parker 1975). However, when this toroidal field emerges through the surface of the Sun, the magnetic flux tubes are oriented in a primarily radial direction in the photosphere (e.g. see the review by Solanki 2009).

Stars with masses below $\sim 0.35 M_{\odot}$ ($\sim M3$) are expected to be fully convective as suggested by standard models (e.g., Chabrier & Baraffe 1997). This limit probably shifts toward lower masses due to the influence of the magnetic field (Mullan & MacDonald 2001; Chabrier et al. 2007). In fully convective stars, the lack of a radiative core is expected to preclude the $\alpha\Omega$ dynamo, maintained by the combined action of differential rotation (Ω effect) and cyclonic convection (α effect). This raises the question of what type of dynamo produces strong magnetic activity as observed in mid to late M and brown dwarfs from photospheric Zeeman splitting (Johns-Krull & Valenti 1996; Reiners & Basri 2007) to chromospheric H α and Ca II IRT (Liebert et al. 2003; Phan-Bao et al. 2006; Schmidt et al. 2007), coronal X-ray (Audard et al. 2007; Stelzer et al. 2006; Robrade et al. 2009), and radio (Berger 2002; Phan-Bao et al. 2007; Berger et al. 2008; Hallinan et al. 2008; Osten et al. 2009) emissions.

An alternative dynamo known as the so-called α^2 dynamo maintained by convection alone was proposed (Roberts & Stix 1972). It has been developed for fully convective pre-main sequence stars (Schüssler 1975;

¹ Based on observations made at the Canada-France-Hawaii Telescope, operated by the National Research Council of Canada, the Centre National de la Recherche Scientifique de France and the University of Hawaii.

² Institute of Astronomy and Astrophysics, Academia Sinica, P.O. Box 23-141, Taipei 106, Taiwan, ROC; pbn-goc@asiaa.sinica.edu.tw; jlim@asiaa.sinica.edu.tw.

³ Department of Physics, HCMIU, Vietnam National University Administrative Building, Block 6, Linh Trung Ward, Thu Duc District, HCM, Vietnam.

⁴ Department of Physics, Room 518, Chong Yuet Ming Physics Building, The University of Hong Kong, Pokfulam Road, Hong Kong, China.

⁵ Laboratoire d'Astrophysique, Observatoire Midi-Pyrénées, F-31400 Toulouse, France; donati@ast.obs-mip.fr.

⁶ Department of Physics and Astronomy, Rice University, 6100 Main Street, MS-61 Houston, TX 77005; cmj@rice.edu.

⁷ CSIC-INTA Centro de Astrobiología, Torrejón de Ardoz, Madrid, Spain; ege@iac.es.

⁸ University of Central Florida, Dept. of Physics, PO Box 162385, Orlando, FL 32816-2385.

Rüdiger & Elstner 1994; Küker & Rüdiger 1997, 1999) and late M dwarfs and brown dwarfs (Dobler et al. 2006; Chabrier & Küker 2006; Browning 2008). In general, these models predict large-scale fields, and magnetic field detections are now known for a number of active objects in these groups (Saar 1994; Johns-Krull & Valenti 1996; Donati et al. 2006a; Morin et al. 2008; Berger et al. 2009). However, the models disagree with each other on the magnetic field morphology and they disagree with the results from some phase-resolved spectropolarimetric observations (Donati et al. 2006a; Morin et al. 2008). For example, the latest dynamo simulations (Browning 2008) successfully predict that the magnetic fields possess large-scale fields with a lack of differential rotation in rapidly rotating M dwarfs. However, the simulations predict the field morphology in fully convective stars should be mostly toroidal, whereas results of Donati et al. (2006a) and Morin et al. (2008) show dominantly poloidal fields in 5 M3-M4.5 dwarfs.

In this paper, we present our mapping of the M4 dwarf G 164-31 based on 20 hours of spectropolarimetric observations spread over 3 successive nights. To date, there are only two M4 dwarfs (V374 Peg, Donati et al. 2006a; G 164-31, this paper) that have been densely monitored over only a few rotation cycles so as to preclude intrinsically long-term magnetic variability, which can affect the mapping result. In addition, for the first time a synthetic spectrum fitting technique (Marcy 1982; Saar 1988; Johns-Krull & Valenti 1996) is applied for measuring the mean field strength and the filling factor in G 164-31. Together, the polarimetric field mapping and the mean field measurements provide us a better accounting of both large- and small-scale fields in one of these two rapid rotators. We also present our Zeeman signature search in Stokes V for 5 other M-dwarfs with spectral types ranging from M0 to M4.5: Gl 890 (M0V), LHS 473 (M2.5V), KP Tau (M3V), Gl 896B (M4.5V) and 2E 4498 (M4.5V). Strong circular polarization is detected in KP Tau, Gl 896B and 2E 4498.

We present our targets in § 2 and the observation and the data reduction in § 3. We apply the tomographic imaging technique for constructing the field topology of Gl 490B in § 4. We discuss the field topology of the 6 M dwarfs in § 5 and summarize the results in § 6.

2. TARGETS

2.1. Targets

All the 6 targets have spectral types from M0V to M4.5V and their physical parameters are listed in Table 1. From our mass estimates (see Table 1 and references therein), three M dwarfs (KP Tau, G 164-31 and 2E 4498) have masses estimated below $0.35 M_{\odot}$ (or absolute magnitudes fainter than $M_K = 6.62$) and are expected to be fully convective according to standard models. Two early-M dwarfs (Gl 890 and LHS 473) are partially convective. The absolute magnitude of the unresolved binary system Gl 896Bab is $M_K = 7.28$, which gives $M_K > 7.28$ for each companion. Both components are therefore expected to be fully convective.

2.1.1. Gl 890 (HK Aqr), M0V

This flaring M0 dwarf is a rapid rotator with $v \sin i = 70 \text{ km s}^{-1}$ (Young et al. 1984). A photometric period of

0.431 days was determined by Young et al. (1990). The star has been well studied for magnetic activity, but no circular polarization observations have been reported so far. Rao & Singh (1990) detected a steady soft X-ray emission from the source, indicating coronal activity. Its X-ray luminosity (0.2-4.5 keV) was measured by XMM-Newton at $\log L_X (\text{ergs s}^{-1}) \approx 29.0$ (XMM-SSC 2008). A large flarelike event was also detected by Singh et al. (1999) from the X-ray light curve. Gl 890 was observed with the Australia Telescope Compact Array (ATCA) at 6 cm over the full rotation phase in 1990, but the source was not detected at an upper flux limit of $\approx 0.3 \text{ mJy}$ (Lim 1993). It was subsequently detected as a weak (below 0.3 mJy) slowly varying source with the Very Large Array (VLA) (Lim 1993, quoting a private communication by M. Güdel & A. D. Benz 1992).

2.1.2. LHS 473 (GJ 752A), M2.5V

LHS 473 is an M2.5 dwarf, a companion of VB 10 (M8), and has a low rotational velocity $v \sin i < 2.6 \text{ km s}^{-1}$ (Delfosse et al. 1998). Vaiana et al. (1981) reported a soft X-ray (0.2-4.0 keV) detection with $\log L_X = 27.11$. Leto et al. (2000) carried out VLA radio observations but the star was not detected in all 4 different observed radio bands. These observations indicate a low coronal activity level in LHS 473. Stauffer & Hartmann (1986) also reported weak chromospheric activity with an H α absorption equivalent width of 0.35 \AA (Cram & Giampapa 1987). Johns-Krull & Valenti (1996) classified LHS 473 an inactive M dwarf.

2.1.3. KP Tau (Wolf 1246, RX J0339.4+2457), M3V

This M3 dwarf, in contrast with LHS 473, is a rapid rotator with $v \sin i = 32 \text{ km s}^{-1}$ (Mochneck et al. 2002). The dwarf is a ROSAT source (0.1-2.4 keV) with $\log L_X = 28.13$ (Fleming 1998; Hünsch et al. 1999), implying that the coronal activity level in KP Tau is over an order of magnitude higher than that in LHS 473 (which has a similar spectral type). To date, no radio observations of the star have been reported.

2.1.4. G 164-31 (Gl 490B), M4V

G 164-31 is a star with a spectral type of M4V (Reid et al. 1995) at a distance of 18.1 pc (ESA 1997), which is the companion of G 164-32 (Gl 490A, M0.5V) at a large angular separation of $15''$. At the given distance and its apparent 2MASS K -band magnitude of $K = 8.02$, we derive its absolute magnitude $M_K = 6.73$. This fast rotator with $v \sin i = 34 \text{ km s}^{-1}$ exhibits high coronal activity in X-ray emission (0.3-3.5 keV) with $\log L_X = 29.05$ (Fleming et al. 1989). No radio observations of the star have been reported to date. Using the Segransan et al. (2003) empirical relationship of M_K versus radius, we derive $R_{\star} = 0.34 R_{\odot}$, which is in good agreement with theoretical models (e.g., Baraffe et al. 1998) for inactive dwarfs (see Demory et al. 2009). This estimated radius yields a maximum rotational period of ~ 12.1 hours.

2.1.5. Gl 896B (EQ Peg B), M4.5V

The Gl 896 system is a quadruple Gl 896AabBab (Delfosse et al. 1999; Oppenheimer et al. 2001). Gl 896 Bab is a single-lined spectroscopic binary with a joint spectral type of M4.5 and a joint $v \sin i$ of 24.2 km s^{-1}

(Delfosse et al. 1998). Gl 896Bab was detected at radio frequencies (Güdel et al. 1993) of 4.9 GHz (6 cm) and 8.5 GHz (3.6 cm). The joint X-ray luminosity (0.1-2.4 keV) of the Gl 896 AabBab system is $\log L_X = 28.84$ (Güdel et al. 1993). Robrade et al. (2009) reported Gl 896Bab was on average a factor of 3.5 weaker than Gl 896Aab, we therefore derive $\log L_X = 28.19$ for Gl 896Bab.

2.1.6. 2E 4498 (RX J2137.6+0137), M4.5V

No spectral type estimate of this dwarf is available in the literature. From our unpolarized (Stokes I) spectra obtained with ESPaDOnS (see § 3.1), using a spectral index versus spectral type relationships for M dwarfs (e.g., Martín et al. 1999), we estimate its spectral type as $M4.5 \pm 0.5$, giving it an absolute magnitude $M_I \approx 10.1$ (e.g., Leggett 1992). Comparison with the DENIS apparent magnitude $I = 10.38$ (Epchtein 1997) then gives a distance of ~ 11.4 pc, assuming no reddening. The source shows coronal activity in X-ray emission (0.1-2.4 keV) with a measured flux $f_X = 4.52 \times 10^{-12}$ ergs s^{-1} cm^{-2} and 20 cm radio emissions (see Brinkmann et al. 2000 and references therein). At the source distance, we derive $\log L_X = 28.85$. The radius of an M4.5 dwarf is about $0.3 R_\odot$ (Chabrier & Baraffe 1997), resulting in a maximum rotational period of 7.5 hours at $v \sin i = 55$ km s^{-1} (Mochnecki et al. 2002). We detected strong circular polarization in this dwarf (see Fig. 1). Since its rotation period is quite short, our detection makes the source ($M_\star \sim 0.2 M_\odot$) an excellent target for future mapping of the magnetic field on a fully convective star.

3. SPECTROPOLARIMETRIC OBSERVATIONS AND RESULTS

3.1. Observations

We observed the six M dwarfs described above with the Canada-France-Hawaii Telescope's ESPaDOnS high-resolution spectrograph ($R = 65,000$; Donati 2003), which provides a wavelength coverage of 370-1000 nm. The spectropolarimetric mode was used to provide unpolarized (Stokes I) and circularly polarized (Stokes V) spectra. Among the six targets, G 164-31 is a particularly interesting source since it is an analog of V374 Peg (G 188-38), which is a rapidly rotating M4 dwarf with $v \sin i \approx 37$ km s^{-1} showing a large-scale poloidal field (Donati et al. 2006a). G 164-31 is therefore also an excellent target on which to study the field topology in fully convective stars.

Each observation consists of 4 exposures taken at different polarimeter configurations and combined together to filter out spurious polarization signatures to first order (Donati et al. 1997a). Exposure times were computed using the exposure time calculator for ESPaDOnS to obtain signal-to-noise ratios above 100 at the wavelengths of interest. This signal-to-noise value is typical of what is needed to detect the circular polarization in M dwarfs (e.g., Phan-Bao et al. 2006). In the case of G 164-31, we monitored the star for a total of 20 hours from 2008 March 23 to 26 with 33 observations, aiming to cover at least one full rotation period of the star. The full observing logs are given in Table 2.

Data reduction was performed using Libre-ESpRIT (Donati et al. 1997a) utilizing the principles of opti-

mal extraction as given in Horne (1986). As the Zeeman signature is typically very weak, several methods (Semel et al. 2008; Martínez González et al. 2008; Donati et al. 1997a) have been used in the past to increase the signal-to-noise ratio of Zeeman signatures. In this work, the Least-Squares Deconvolution (LSD, Donati et al. 1997a) multi-line analysis procedure was applied to the spectra to extract the polarization signal from a large number of photospheric atomic lines⁹ and compute a mean Zeeman signature corresponding to an average photospheric profile centered at 700 nm. Both mean Stokes I and V profiles are computed for all collected spectra. Figure 1 shows the LSD Stokes I and V profiles of KP Tau, Gl 896B and 2E 4498 in which we detect Zeeman signatures. The profiles of G 164-31 are shown in Figures 2 and 3. Using the basic equations listed in Wade et al. (2000) (see also Brown & Landstreet 1981; Donati et al. 1997a), we compute the net longitudinal magnetic field strength, B_z , from our LSD Stokes I and V profiles. In the case of G 164-31, its time series of Stokes I and Stokes V profiles are used in the following section to reconstruct the field topology on this M4 dwarf.

3.2. Results

Table 1 lists our measurements of B_z for all targets. We detected strong Zeeman signatures in KP Tau, G164-31, Gl 896B and 2E 4498 but we did not detect them in the two early-M dwarfs Gl 890 and LHS 473. The photospheric field strength is estimated from LSD Stokes I and V profiles, and the chromospheric field is computed from the Stokes profiles of only the H α line.

For G 164-31, we find that the Zeeman signatures repeat after 0.540 ± 0.006 day (12.96 ± 0.14 hours), which is in the expected range of its rotation period. We thus conclude that the rotation period of this dwarf is 12.96 hours. We note that this value is slightly greater than the estimated maximum rotation period of 12.1 hours for this star. The difference is possibly due to G 164-31 having a larger radius than the expected value from theory. Matching unpolarized (Stokes I) spectra of G 164-31 with that of slowly rotating references requires a projected rotation velocity of $v \sin i = 41 \pm 1$ km s^{-1} . Our value is greater than one of Fleming et al. (1989), $v \sin i = 34 \pm 8.5$ km s^{-1} , though both measurements are consistent to within the uncertainties. Dues to its smaller uncertainty, we adopt our $v \sin i = 41$ km s^{-1} for G 164-31. From P_{rot} and $v \sin i$, we derive $R \sin i = 0.44 \pm 0.02 R_\odot$. Our $R \sin i$ is $\sim 30\%$ larger than the estimated stellar radius (see § 2.1.4). It is unlikely that it exactly equals 90° , and the results obtained in the imaging process described below are similar for $60^\circ \leq i \leq 80^\circ$. We thus set $i = 70^\circ$, which results in the G 164-31 radius being $\sim 38\%$ larger than the typical value for M dwarfs of the same luminosity. This is likely due to the fact that G 164-31 is a

⁹ We used a line list (Kurucz 1993) corresponding to M spectral types matching that of the six dwarfs. Approximately 5000 intermediate to strong atomic spectral lines with an average Landé factor g_{eff} of ~ 1.2 are used simultaneously to retrieve the average polarization information with typical noise levels of $\approx 0.08\%$ (relative to the unpolarized continuum level) per 1.8 km s^{-1} velocity bin and per individual polarization spectrum. This represents a multiplex gain in S/N of about 10 with respect to a single line analysis.

young object belonging to a moving cluster identified by Orlov et al. (1995). We refer the reader to § 5 for further discussion.

We monitored G 164-31 for 20 hours spread over three successive nights, aiming for coverage over a full rotational cycle. The true period (12.96 hours) is a bit longer than our expected maximum value (12.1 hours). With this period, our observations cover only half of the rotational phase. In other words, only half of the stellar surface was monitored. A few of the Stokes I and V LSD profiles are discarded due to the contamination of moonlight or flaring events. Figure 2 and 3 show Stokes I and V LSD profiles of G 164-31.

4. MODELING OF MAGNETIC FIELD TOPOLOGY OF G 164-31

To reconstruct the map of cool spots and magnetic fields at the surface of G 164-31 from the set of observed LSD Stokes I and V , we use the Donati et al. (2001) magnetic mapping code which employs the Zeeman-Doppler imaging (ZDI) technique (Semel et al. 1989). The typical longitude resolution achieved at the equator is $\approx 15^\circ$ or ≈ 0.04 rotation cycle. The basic idea of the code has been fully described in several papers (Brown et al. 1991; Donati et al. 1997b, 2001, 2006b; Morin et al. 2008). In this paper, we briefly describe the principles of the modeling work and refer the reader to the above papers for further details.

4.1. Mapping spots

Cool spots on the surface of a rapidly rotating star produce distortions in the stellar spectral lines. If the star is rotating fast enough (at least 20-30 km s⁻¹ for late-type dwarfs, Vogt et al. 1987), the shape of the star's spectral line profiles are dominated by rotational Doppler broadening. In this case, there is a strong correlation between the position of any distortion within a line profile and the position of the corresponding spot on the stellar surface. A spectrum of the rapid rotator is a one-dimensional image that is resolved in the direction perpendicular to the stellar rotation axis and the light-of-sight. By observing the star at different rotation phases, a two-dimensional image of the spot distribution can be reconstructed using the so-called Doppler imaging (DI) technique (see Vogt et al. 1987 and references therein). In the imaging process, the stellar surface is divided into a grid of 1000 elementary cells. Using the spot-occupancy model of Cameron (1992), the local line profile at each grid point of the surface is described as a linear combination of two reference profiles, one representing the quiet photosphere and one for cool spots. Both reference profiles are assumed to be equal and only differ by their relative continuum levels. For the assumed reference profile, we can use either the LSD profile of the very slowly rotating inactive M4 dwarf G1 402 or a simple Gaussian profile with similar full width at half-maximum and equivalent width. Both options yield very similar results, indicating that the exact shape of the assumed local profiles has very minor impact on the reconstructed images, as long as the rotational velocity of the star is much larger than the local profile. Each element on the surface is quantified by the local fraction occupied by spots. The spot occupancy ranges from 0 (no spots) to 1 (complete spot coverage). The maximum entropy image reconstruction

technique (Skilling & Bryan 1984; Vogt 1980) is used to find the image having the smoothest variation (or in some sense the simplest image), giving the least contrast between spots and the quiet photosphere.

4.2. Mapping magnetic fields

The field is described as the sum of a poloidal and a toroidal component, both expressed as spherical harmonics expansions (Jardine et al. 1999). For a given set of the complex coefficients of the spherical harmonic expansions, one can produce a corresponding topology (or a Stokes V data set) at the stellar surface. The code uses the maximum entropy image reconstruction technique, in which entropy (i.e., quantifying the amount of reconstructed information) is calculated from the coefficients of the spherical harmonics expansions. The imaging process starts from a null magnetic field and iteratively adjusts the spherical harmonic coefficients in order to match the synthetic Stokes V profile to the observed LSD one. The code uses a multidirectional search in the image space until the required maximum entropy image is obtained. This corresponds to an optimal field topology that reproduces the data at a given χ^2 level, i.e., usually down to noise level. Since the inversion problem is partially ill posed, we use the entropy function to select the magnetic field map with lowest information content among all those reproducing the data equally well.

To calculate the synthetic Stokes V profiles for a given field topology, the surface was again divided into a grid of 1000 elementary surface cells. In each cell, the three components (radial, azimuthal and meridional in spherical coordinates) of the vector field are estimated directly from the spherical harmonic expansion. The code uses the analytic solutions (Landolfi & Landi Degl'Innocenti 1982) of Unno-Rachkovsky's radiative transfer equations to calculate the contribution to the Stokes V profiles of all visible cells at each observed rotation phase. The free parameters in the Unno-Rachkovsky equations are obtained by fitting the LSD Stokes I profile of a very slowly rotating and weakly active star with a similar spectral type (e.g., G1 402). To obtain the best fit (in both amplitude and width) between the synthetic and observed Stokes V profiles, the code introduces a filling factor f_c , which represents the fractional amount of circular flux being constant over the whole stellar surface, and speculates that large-scale fields in M dwarfs can be structured on a small scale (Donati et al. 2008). The circularly polarized flux from each cell is thus $f_c V_{\text{loc}}$, where V_{loc} is the Stokes V profile derived from the analytic solutions of the Unno-Rachkovsky equations.

Differential rotation is also implemented in the calculation process of the synthetic Stokes V profiles for yielding the best fits to the observation. For this purpose, we assume the rotation rate varies with latitude, θ , following a solar-like differential rotation law as $\Omega(\theta) = \Omega_{\text{eq}} - d\Omega \sin^2\theta$, where Ω_{eq} is the angular rotation rate at the equator, and $d\Omega$ is the difference in angular rotation rate between the equator and the pole. Differential rotation is detected when χ^2 of the fit to the data shows a well defined minimum in the range of Ω_{eq} and $d\Omega$ values. In the case of G 164-31, we did not obtain a clear minimum in the explored $\Omega_{\text{eq}} - d\Omega$ range. This indicates that our data are not suitable for measuring differential rotation given the fairly simple (and low amplitude) rotational

modulation of the Stokes V profiles we observe. This is mostly due to the fact that the field distribution lacks well defined features at different latitudes from which differential rotation can be estimated. Based on the previous observations of analogs of G 164-31 (Donati et al. 2006a; Morin et al. 2008), we therefore assumed that this star rotates as a rigid body while performing the field mapping. The obtained map of G 164-31 is shown in Figure 4.

4.3. Results

Figure 4 presents our maps of the spot occupancy and the magnetic field at the stellar surface of G 164-31. For the half stellar surface that was not observed, the field topology has been derived using a spherical harmonic expansion based on the collected Stokes V data set. Our brightness map shows a low contrast spot at the pole of the star. The magnetic field morphology on G 164-31 shows that the radial field component is dominant, which appears similar to what is seen in V374 Peg. The azimuthal and meridional components are negligible.

The average large-scale flux is 680 G and the poloidal field dominates with 99% of the energy content. Most (95%) of this poloidal field is stored in the mode corresponding to a dipole aligned with the rotation axis (spherical harmonics degree $l = 1$ and order $m = 0$). One should note that due to the high $v \sin i$ of G 164-31, for any value of the filling factor $0 < f_c < 1$, we find similar results. Hence, we arbitrarily set $f_c = 1$. We also examine the binarity of G 164-31. Based on the LSD Stokes I profiles, we find an average radial velocity value of $-6.7 \pm 0.2 \text{ km s}^{-1}$. No significant variation in radial velocity is found. Therefore, our current data does not reveal any hint of an additional close-in component around G 164-31.

5. DISCUSSION

In this section, we first briefly discuss the magnetic field properties of the stars whose fields are not mapped. These stars are Gl 890, LHS 473, KP Tau, Gl 896B and 2E 4498. We then focus the discussion on the field topology in the photosphere and the chromosphere of G 164-31.

5.1. Individual stars: Gl 890, LHS 473, KP Tau, Gl 896B and 2E 4498

We did not detect Zeeman signatures in Gl 890 and LHS 473. For the latter case, the non-detection in both the photosphere and the chromosphere indicates that LHS 473 is inactive, likely due to its low $v \sin i$, and this result is consistent with previous observations showing its low coronal activity level. However in the fastly rotating case of Gl 890, the non-detection suggests that the field topology on this star may be different from what has been observed in more slowly-rotating early-M dwarfs (Donati et al. 2008), whose fields are large-scale and dominantly toroidal producing Stokes V signatures detectable at any time. Since the detections of X-ray and radio emission indicate that Gl 890 is magnetically active, phase-resolved spectropolarimetric observations of this star are therefore needed to clarify its magnetic field topology.

For the three remaining M dwarfs, all these fast rotators show Zeeman signatures, and they are particularly

strong in Gl 896B and 2E 4498 (Fig. 1). This result indicates the presence of strong, large-scale fields on these stars. Since KP Tau ($0.31 M_{\odot}$) and 2E 4498 ($0.21 M_{\odot}$) are fully convective, they are good targets for studying the field morphology by carrying out spectropolarimetric and simultaneous multiple-wavelength observations (e.g., Berger et al. 2009). We note that Gl 896Bab is an unresolved binary. Therefore, its Zeeman signature is contributed by two components if both are magnetically active.

5.2. G 164-31

The G 164-31 magnetic field topology, which is mostly poloidal with most of the magnetic energy concentrated within the lowest order axisymmetric modes, is very similar to what has been observed in V374 Peg (Donati et al. 2006a) and other mid-M dwarfs (Morin et al. 2008). The average large-scale magnetic flux on G 164-31 is 0.68 kG, which is significantly smaller than the previous measurements of few kiloGauss magnetic fluxes in active mid-M dwarfs using synthetic spectrum fitting techniques (e.g., Johns-Krull & Valenti 1996). This is possibly due to the ZDI technique being sensitive to only large-scale and simple structures, while Zeeman signatures from magnetic regions with complicated or small-scale topology may cancel each other in circularly polarized spectra whereas these signatures add up in unpolarized spectra. To explore this “missing” magnetic flux, we used the synthetic spectrum fitting technique described in Johns-Krull & Valenti (1996) to measure the mean magnetic flux on the surface of G 164-31. Briefly, spectra in the wavelength interval around the Zeeman-sensitive Fe I line at 8468.40 \AA are analyzed. In stars as cool as G 164-31, this line is actually blended with a Ti I line at 8468.47 \AA which is similar in strength and also Zeeman sensitive. The spectrum synthesis models both lines plus numerous TiO lines in this wavelength region. Because of the ubiquitous TiO, spectral changes due to magnetic fields are seen more clearly in the ratio of active to inactive line profiles. Therefore, spectra of G 164-31 were divided by inactive references. In our case, we used two inactive reference stars GJ 725B (or LHS 59, M3.5V) and GJ 876 (or LHS 530, M4V) which are meant to be identical in all respects (T_{eff} , $\log g$, $[M/H]$, etc.) to G 164-31 except for the field. Line profiles were synthesized with and without magnetic fields (see Johns-Krull & Valenti 1996 and references therein) and the ratio of active to inactive profiles was fit by adjusting the magnetic field strength, B , and its filling factor, f , in the model spectrum of G 164-31. The line profiles are generated assuming a uniform radial field everywhere with a uniform filling factor.

The best fits were obtained with $Bf = 3.1 \text{ kG}$ and $Bf = 3.3 \text{ kG}$ for GJ 725B and GJ 876. The fit to the observations using GJ 876 as the inactive reference star is shown in Figure 5. Due to the high $v \sin i$ of G 164-31, we can not measure B and f separately. The model fit in the line core is not as good as we would like, and is only slightly improved using GJ 725B as the reference star. We note though that if the radius of G 164-31 is indeed larger than expected due to youth (see below), its gravity is likely somewhat lower than that of either inactive comparison star. Our spectrum synthesis indicates that the 8468 \AA feature should actually weaken somewhat at

lower gravity, which would result in the discrepancy in the core getting worse by ~ 0.005 in the ratio. A possible way to correct for this would be to fit a distribution of magnetic field strengths on the stellar surface as has been done for M dwarfs (Johns-Krull & Valenti 2000) and on T Tauri stars (e.g. Johns-Krull et al. 1999). The current fit (Fig. 5) attempts to use a single field strength to fit both the wings and the core, whereas a distribution of magnetic fields gives more flexibility in fitting the entire profile and can result in bigger changes in the line equivalent width than produced when using only a single field value. We therefore adopt $Bf = 3.2 \pm 0.4$ kG for G 164-31 as the best estimate from our single field fitting described above, noting that this may be a slight underestimate. This value for Bf is larger than the one measured from the ZDI technique by a factor of 4.7. Our result is consistent with the previous measurements from the literature (e.g., EV Lac, Johns-Krull & Valenti 1996; Morin et al. 2008), suggesting that in active mid-M dwarfs a significant part of the magnetic energy is stored in small-scale structures. As found by Reiners & Basri (2007), it appears that a large majority of the magnetic energy is stored in the small scale field of G 164-31. Apparently, a successful dynamo model should be able to produce both large-scale poloidal fields and small-scale features in rapidly rotating mid-M dwarfs.

To study chromospheric activity, we computed the $H\alpha$ emission equivalent widths for each exposure. Our $H\alpha$ emission light curve is shown in Fig. 6. One should keep in mind that since each observation to obtain a Stokes V profile consists of 4 exposures, measuring $H\alpha$ emission at individual exposures therefore increases time resolution of the light curve. Figure 6 also indicates that the $H\alpha$ equivalent width variations are likely sinusoidal and they are modulated by the stellar rotation with $P_{\text{rot}} = 0.54$ day determined from the Stokes V profiles. This effect has also been observed in late-M and brown dwarfs (see Berger et al. 2009 and references therein). Flaring events were seen strongly in the last sequences of the first observing night and moderately in the middle sequences of the second night. These events were also observed in the $H\beta$ emission profiles. While the likely rotational modulation and nonzero minimum of the $H\alpha$ light curve imply either a large-scale (poloidal or toroidal) chromospheric field or a localized concentration of small-scale magnetic activity, it is reasonable to assume that the chromospheric field in G 164-31 has both a large scale poloidal component and small-scale structures as observed in the photospheric field. This field configuration probably dominates in both the photosphere and the chromosphere of the star. We note that simultaneous observations at multiple wavelengths of the source will place more constraints on the chromospheric and coronal field morphology (e.g., Berger et al. 2009).

It is very interesting to note that the radius of G 164-31 is at least 30% larger than that estimated from standard models for M dwarfs at the same luminosity (see § 2.1.4). There are two possible interpretations of this discrepancy. First, the magnetic field effects of reduced convective efficiency due to fast rotation and large field strengths, and/or to spot coverage as proposed by Chabrier et al. (2007) might yield a cooler effective temperature T_{eff} and thus a larger radius in low-mass stars, keeping their luminosity unchanged ($L \propto T_{\text{eff}}^4 R^2$).

Our spot mapping (Fig. 4) shows the fraction of the stellar surface covered by the low contrast spot is relatively small in G 164-31. However, one should note that the imaging technique is only sensitive to spots or spot groups with sizes comparable to our resolution element. We therefore can not rule out the possibility of unresolved small spots spread everywhere on the stellar surface. Hence, we can not conclude whether the effect due to spot coverage is significant in this star or not. Observational results (see Ribas 2006; Morales et al. 2008 and references therein) suggest that these effects might yield a $\sim 10 - 15\%$ larger radius in G 164-31, therefore the discrepancy in radius of over 30% can not be explained by only those effects. Second, we explore the possibility that G 164-31 is a young M4 dwarf, its radius thus larger than one computed for old M dwarfs. We note that the K -band absolute magnitude of G 164-31, $M_K = 6.73$, is 0.67 mag brighter than the average value for M4 dwarfs¹⁰, supporting the young nature of the star. From a literature search, the binary system G 164-31 (Gl 490B)+G 164-32 (Gl 490A) indeed belongs to a moving cluster previously identified by Orlov et al. (1995) (for a review on young nearby stars, see Zuckerman & Song 2004). One should note that the primary component G 164-32 also exhibits high coronal X-ray emission with $\log(L_X/L_{\text{bol}}) = -3.23$ (Fleming et al. 1989) and chromospheric $H\alpha$ emission (Stauffer & Hartmann 1986), indicating activity typical in young early-M dwarfs. We measured an upper limit for the Li $\lambda 6708$ equivalent width of 17 mÅ for G 164-31. This gives the star an age older than 10 Myr since early-M dwarfs ($\geq M4$) are expected to completely deplete their Lithium within ~ 10 Myr. We suggest G 164-31 is an analog of the M4 dwarf HIP 112312A at 23.6 pc (ESA 1997), which is a member of the ~ 12 Myr old β Pictoris moving group (Song et al. 2002). To estimate the mass and age of G 164-31, we used the Chabrier et al. (2007); Baraffe et al. (1998) theoretical models with constraints of $M_K = 6.73$, $I - J = 1.61$, and the deduced radius $R_* = 0.47 R_{\odot}$ of G 164-31, and we also considered the magnetic field effects that might yield about a 10-15% larger radius. We then derived $M_* \sim 0.15 M_{\odot}$ at an age of about 25-30 Myr, making G 164-31 the least massive M dwarf whose magnetic field has been mapped to date. More observations are needed to precisely determine the fundamental parameters of this moving cluster.

6. SUMMARY

Based on our circularly polarized and unpolarized spectroscopic observations, using both tomographic imaging and synthetic spectrum fitting, we reveal the mainly axisymmetric large-scale poloidal magnetic field and the small-scale field structures storing a significant portion of the magnetic energy in the photosphere of the M4 dwarf G 164-31. The modulation of the $H\alpha$ emission light curve suggests that the field in the chromosphere is stable and possibly poloidal like that in the photosphere. Our detection of circular polarization in the single and rapidly rotating M dwarfs KP Tau (M3V), 2E 4498

¹⁰ We selected 9 single M4 dwarfs within 10 pc listed in Delfosse et al. (1998) and computed their K -band absolute magnitude from trigonometric parallaxes and 2MASS K -band magnitudes available in the VIZIER database. This work yielded an average value $M_K = 7.4$.

(M4.5V) make them good targets for mapping of the field morphology in mid-M dwarfs in the future.

N. P.-B. has been aided in this work by a Henri Chretien International Research Grant administered by the American Astronomical Society. E. M. acknowledges support from the Spanish Ministry of Science through

the project AYA2007-67458. The authors extend special thanks to those of Hawaiian ancestry on whose sacred mountain we are privileged to be guests. Access to the CFHT was made possible by the Ministry of Education and the National Science Council of Taiwan as part of the Cosmology and Particle Astrophysics (CosPA) initiative.

REFERENCES

- Audard, M., Osten, R. A., Brown, A., Briggs, K. R., Güdel, M., Hodges-Kluck, E., & Gizis, J. E. 2007, *A&A*, 471, L63
- Baraffe, I., Chabrier, G., Allard, F., & Hauschildt, P. H. 1998, *A&A*, 337, 403
- Berger, E. 2002, *ApJ*, 572, 503
- Berger, E., et al. 2008, *ApJ*, 676, 1307
- Berger, E., et al. 2009, *ApJ*, 695, 310
- Brinkmann, W., Laurent-Muehleisen, S. A., Voges, W., Siebert, J., Becker, R. H., Brotherton, M. S., White, R. L., & Gregg, M. D. 2000, *A&A*, 356, 445
- Brown, D. N., & Landstreet, J. D. 1981, *ApJ*, 246, 899
- Brown, S., Donati, J.-F., Rees, D., & Semel, M. 1991, *A&A*, 250, 463
- Browning, M. K. 2008, *ApJ*, 676, 1262
- Cameron A., 1992, in *Lecture Notes in Physics 397, Surface Inhomogeneities on Late-Type Stars*, ed. P. B. Byrne & D. J. Mullan (Berlin: Springer-Verlag), 33
- Chabrier, G., & Baraffe, I. 1997, *A&A*, 327, 1039
- Chabrier, G., & Küker, M. 2006, *A&A*, 446, 1027
- Chabrier, G., Gallardo, J., & Baraffe, I. 2007, *A&A*, 472, L17
- Cram, L. E., & Giampapa, M. S. 1987, *ApJ*, 323, 316
- Delfosse, X., Forveille, T., Perrier, C., & Mayor, M. 1998, *A&A*, 331, 581
- Delfosse, X., Forveille, T., Beuzit, J.-L., Udry, S., Mayor, M., & Perrier, C. 1999, *A&A*, 344, 897
- Delfosse, X., Forveille, T., Ségransan, D., Beuzit, J.-L., Udry, S., Perrier, C., & Mayor, M. 2000, *A&A*, 364, 217
- Demory, B.-O., et al. 2009, *A&A*, in press (arXiv:0906.0602)
- Dobler, W., Stix, M., & Brandenburg, A. 2006, *ApJ*, 638, 336
- Donati, J.-F., Semel, M., Carter, B. D., et al. 1997a, *MNRAS*, 291, 658
- Donati, J.-F., & Brown, S. F. 1997b, *A&A*, 326, 1135
- Donati, J.-F., Wade, G. A., Babel, J., Henrichs, H. F., de Jong, J. A., & Harries, T. J. 2001, *MNRAS*, 326, 1265
- Donati, J.-F. 2003, in *ASP Conf. Ser. 307, Solar Polarization*, ed. J. Trujillo-Bueno & J. Sanchez Almeida (San Francisco: ASP), 41
- Donati, J.-F., Forveille, T., Cameron, A. C., Barnes, J. R., Delfosse, X., Jardine, M. M., & Valenti, J. A. 2006a, *Science*, 311, 633
- Donati, J.-F., et al. 2006b, *MNRAS*, 370, 629
- Donati, J.-F., et al. 2008, *MNRAS*, 390, 545
- Durney, B. R., De Young, D. S., & Roxburgh, I. W. 1993, *Sol. Phys.*, 145, 207
- Epchtein, N. 1997, in *Garzon F., Epchtein N., Omont A., Burton B., Persi P., eds, The impact of large scale near-IR sky surveys*, Kluwer Academic Publishers, Dordrecht, p. 15
- ESA 1997, *The Hipparcos and Tycho Catalogues*, ESA SP-1200
- Fleming, T. A., Gioia, I. M., Maccacaro, T. 1989, *ApJ*, 340, 1011
- Fleming, T. A. 1998, *ApJ*, 504, 461
- Güdel, M., Schmitt, J. H. M. M., Bookbinder, J. A., & Fleming, T. A. 1993, *ApJ*, 415, 236
- Hallinan, G., Antonova, A., Doyle, J. G., Bourke, S., Lane, C., & Golden, A. 2008, *ApJ*, 684, 644
- Horne, K. 1986, *PASP*, 98, 609
- Hünsch, M., Schmitt, J. H. M. M., Sterzik, M. F., & Voges, W. 1999, *A&AS*, 135, 319
- Jardine, M., Barnes, J. R., Donati, J.-F., & Collier Cameron, A. 1999, *MNRAS*, 305, 35
- Johns-Krull, C. M., & Valenti, J. A. 1996, *ApJ*, 459, L95
- Johns-Krull, C. M., & Valenti, J. A. 2000, *Stellar Clusters and Associations: Convection, Rotation, and Dynamos*, 198, 371
- Johns-Krull, C. M., Valenti, J. A., & Koresko, C. 1999, *ApJ*, 516, 900
- Küker, M., & Rüdiger, G. 1997, *A&A*, 328, 253
- Küker, M., & Rüdiger, G. 1999, *A&A*, 346, 922
- Kurucz, R. L. 1993, *CDROM # 13 (ATLAS9 atmospheric models) and # 18 (ATLAS9 and SYNTHE routines, spectral line database)*.
- Landolfi, M., & Landi Degl'Innocenti, E. 1982, *Sol. Phys.*, 78, 355
- Leggett, S. K. 1992, *ApJS*, 82, 531
- Leto, G., Pagano, I., Linsky, J. L., Rodonò, M., & Umana, G. 2000, *A&A*, 359, 1035
- Liebert, J., Kirkpatrick, J. D., Cruz, K. L., Reid, I. N., Burgasser, A., Tinney, C. G., & Gizis, J. E. 2003, *AJ*, 125, 343
- Lim, J. 1992, *ApJ*, 405, L33
- Marcy, G. W. 1982, *PASP*, 94, 989
- Martín, E. L., Delfosse, X., Basri, G., Goldman, B., Forveille, T., & Zapatero Osorio, M. R. 1999, *AJ*, 118, 2466
- Martínez González, M. J., Asensio Ramos, A., Carroll, T.A., Kopf, M., Ramírez Vélez, J. C., & Semel, M. 2008, *A&A*, 486, 637
- Mochnicki, S. W., et al. 2002, *AJ*, 124, 2868
- Morales, J. C., Ribas, I., & Jordi, C. 2008, *A&A*, 478, 507
- Morin, J., et al. 2008, *MNRAS*, 390, 567
- Mullan, D. J., & MacDonald, J. 2001, *ApJ*, 559, 353
- Noyes, R. W., Hartmann, L. W., Baliunas, S. L., Duncan, D. K., & Vaughan, A. H. 1984, *ApJ*, 279, 763
- Oppenheimer, B. R., Golimowski, D. A., Kulkarni, S. R., Matthews, K., Nakajima, T., Creech-Eakman, M., & Durrance, S. T. 2001, *AJ*, 121, 2189
- Orlov, V. V., Panchenko, I. E., Rastorguev, A. S., & Yatsevich, A. V. 1995, *AZh*, 72, 495
- Osten, R. A., Phan-Bao, N., Hawley, S. L., Reid, I. N., & Ojha, R. 2009, *ApJ*, in press (arXiv:0905.4197)
- Parker, E. N. 1975, *ApJ*, 198, 205
- Phan-Bao, N., Martín, E. L., Donati, J.-F., & Lim, J. 2006, *ApJ*, 646, L73
- Phan-Bao, N., Osten, R. A., Lim, J., Martín, E. L., & Ho, P. T. P. 2007, *ApJ*, 658, 553
- Rao, A. R., & Singh, K. P., 1990, *ApJ*, 352, 303
- Reid, I. N., Hawley, S. L., & Gizis, J. E. 1995, *AJ*, 110, 1838
- Reiners, A., & Basri, G. 2007, *ApJ*, 656, 1121
- Ribas, I. 2006, *Ap&SS*, 304, 89
- Roberts, P. H., & Stix, M. 1972, *A&A*, 18, 453
- Robrade, J., & Schmitt, J. H. M. M. 2009, *A&A*, in press (arXiv:0901.3027)
- Rüdiger, G., & Elstner, D. 1994, *A&A*, 281, 46
- Saar, S. H. 1988, *ApJ*, 324, 441
- Saar, S. H. 1994, in *IAU Symp. 154, Infrared Solar Physics*, ed. D. M. Rabin et al. (Dordrecht: Kluwer), 493
- Schmidt, S. J., Cruz, K. L., Bongiorno, B. J., Liebert, J., & Reid, I. N. 2007, *AJ*, 133, 2258
- Schüssler, M. 1975, *A&A*, 38, 263
- Ségransan, D., Kervella, P., Forveille, T., & Queloz, D. 2003, *A&A*, 397, L5
- Semel, M. 1989, *A&A*, 225, 456
- Semel, M., Ramírez Vélez, J. C., Stift, M. J., Martínez González, M. J., López Ariste, A. & Leone, F. 2008, arXiv:0810.3543
- Singh, K. P., Drake, S. A., Gotthelf, E. V., & White, N. E. 1999, *ApJ*, 512, 874
- Skilling, J., & Bryan, R. K. 1984, *MNRAS*, 211, 111
- Solanki, S. K. 2009, *Astronomical Society of the Pacific Conference Series*, 405, 135
- Song, I., Bessell, M., & Zuckerman, B. 2002, *ApJ*, 581, L43
- Stauffer, J. R., & Hartmann, L. W. 1986, *ApJS*, 61, 531
- Stelzer, B., Schmitt, J. H. M. M., Micela, G., & Liefke, C. 2006, *A&A*, 460, 35
- Tinney, C. G., Mould, J. R., & Reid, I. N. 1993, *AJ*, 105, 1045
- Vaiana, G. S., et al. 1981, *ApJ*, 244, 163
- van Altena, W. F., Lee, J. T., & Hoffleit, E. D. 1995, *The General Catalogue of Trigonometric Stellar Parallaxes*, 4th edn. Yale Univ. Observatory, New Haven, CT

- Vogt, S. S. 1980, ApJ, 240, 567
Vogt, S. S., Penrod, G. D., & Hatzes, A. P. 1987, ApJ, 321, 496
Wade, G. A., Donati, J.-F., Landstreet, J. D., & Shorlin, S. L. S. 2000, MNRAS, 313, 851
XMM-SSC 2008, The XMM-Newton 2nd Incremental Source Catalogue (2XMMi), (Leicester, UK: XMM-SSC)
- Young, A., Skumanich, A., & Harlan, E. 1984, ApJ, 282, 683
Young, A., Skumanich, A., MacGregor, K. B., Temple, S. 1990, ApJ, 349, 608
Zuckerman, B., & Song, I. 2004, ARA&A, 42, 685

TABLE 1
PHYSICAL PARAMETERS OF THE 6 M DWARFS

Star	SpT ^a	M_K ^b	$\log L_{\text{bol}}$ ^c (ergs s ⁻¹)	$v \sin i$ ^d (km s ⁻¹)	$\log(R_X)$ ^e	M_\star ^f (M_\odot)	B_z (G)	H α EW (Å)	$B_z(\text{H}\alpha)$ (G)
Gl 890	M0	5.41	32.26	70	-3.26	0.57	<18	0.64±0.01	<22
LHS 473	M2.5	5.83	32.09	<2.6	-4.98	0.48	16±7	-0.29±0.02	<30
KP Tau	M3	6.82	31.66	32	-3.53	0.31	-104±32	0.73±0.05	-580±220
							-92±32	0.73±0.05	210±110
G 164-31	M4	6.73	31.66	41	-2.61	0.33	680 [§]	3.15±0.01 [§]	530±60 [§]
Gl 896B	M4.5	7.28	31.45	24.2	-3.26	0.25	296±40	3.5±0.3	-150±60
							294±37	3.6±0.3	110±60
							279±38	4.8±0.5	160±15
2E 4498	M4.5	7.60	31.31	55	-2.46	0.21	-440±84	4.7±0.5	-270±100

^a Spectral type from the literature.

^b Absolute K -band magnitudes computed from trigonometric parallaxes (Gl 890, LHS 473, G 164-31, Gl 896B) or spectroscopic distances (KP Tau, 2E 4498) and 2MASS K -band magnitudes available in the VIZIER database.

^c Bolometric luminosity estimated using the bolometric correction BC_K versus K -band magnitude relationship in Tinney et al. (1993).

^d Rotational velocity, see text (§ 2.1) for references, except G 164-31 (this paper).

^e $R_X = L_X/L_{\text{bol}}$.

^f Stellar masses estimated using the M_K versus mass empirical relationship in Delfosse et al. (2000).

[§] For G 164-31: the value listed for an average magnetic flux Bf_c computed using the ZDI technique (see § 4.3), assuming $f_c = 1$. Its H α equivalent width and chromospheric field strength B_z are estimated at cycle $E = 0.9181$ where the Zeeman signature appears very strong (see Fig. 3).

TABLE 2
OBSERVING LOGS FOR THE 6 M DWARFS

Target	Date	HJD ^a (2453000+)	UT (h:m:s)	Exposure time (s)	Peak of S/N	Cycle ^b
Gl 890	2007 Sep 29	1372.91386	09:49:13	4×200	166	...
LHS 473	2005 Sep 18	631.74709	05:52:12	4×300	511	...
KP Tau	2007 Sep 29	1373.05187	13:08:24	4×500	153	...
	29	1373.07920	13:47:45	4×500	153	...
Gl 896B	2007 Sep 29	1372.93533	10:18:07	4×300	182	...
	29	1372.95603	10:47:55	4×400	209	...
	29	1373.02336	12:24:53	4×400	195	...
2E 4498	2007 Sep 29	1372.89021	09:15:32	4×500	139	...
G 164-31	2008 Mar 24	1549.80662	07:16:47	4×500	140	0.4937
	24	1549.83227	07:53:43	4×500	144	0.5412
	24	1549.85770	08:30:19	4×500	145	0.5883
	24	1549.88332	09:07:13	4×500	143	0.6358
	24	1549.90865	09:43:42	4×500	140	0.6827
	24	1549.93419	10:20:28	4×500	141	0.7300
	24	1549.95967	10:57:10	4×500	144	0.7772
	24	1549.98510	11:33:47	4×500	145	0.8243
	24	1550.01040	12:10:13	4×500	145	0.8711
	24	1550.03576	12:46:44	4×500	144	0.9181
	24	1550.06109	13:23:13	4×500	149	0.9650
	24	1550.08637	13:59:36	4×500	150	1.0118
	25	1550.87304	08:52:24	4×500	132	2.4686
	25	1550.89882	09:29:31	4×500	138	2.5163
	25	1550.92424	10:06:08	4×500	144	2.5634
	25	1550.94977	10:42:53	4×500	137	2.6107
	25	1550.97519	11:19:29	4×500	140	2.6578
	25	1551.00055	11:56:01	4×500	149	2.7047
	25	1551.02679	12:33:48	4×500	144	2.7533
	25	1551.05210	13:10:15	4×500	145	2.8002
	25	1551.07741	13:46:41	4×500	135	2.8471
	25	1551.10286	14:23:20	4×500	145	2.8942
	26	1551.92059	10:00:51	4×464	138	4.4085
	26	1551.94449	10:35:15	4×464	139	4.4528
	26	1551.96815	11:09:20	4×464	144	4.4966
	26	1551.99187	11:43:30	4×464	127	4.5405
	26	1552.01563	12:17:42	4×464	132	4.5845
	26	1552.04024	12:53:09	4×464	134	4.6301
	26	1552.06392	13:27:14	4×464	141	4.6739
	26	1552.08759	14:01:20	4×464	134	4.7178
	26	1552.11210	14:36:37	4×464	132	4.7631
	26	1552.13587	15:10:51	4×464	114	4.8072
	27	1553.08983	14:04:32	4×464	135	6.5738

^a Heliocentric Julian date (UTC).

^b Rotational cycles E are computed using ephemeris $HJD = 2454549.54 + 0.54E$, only available for G 164-31.

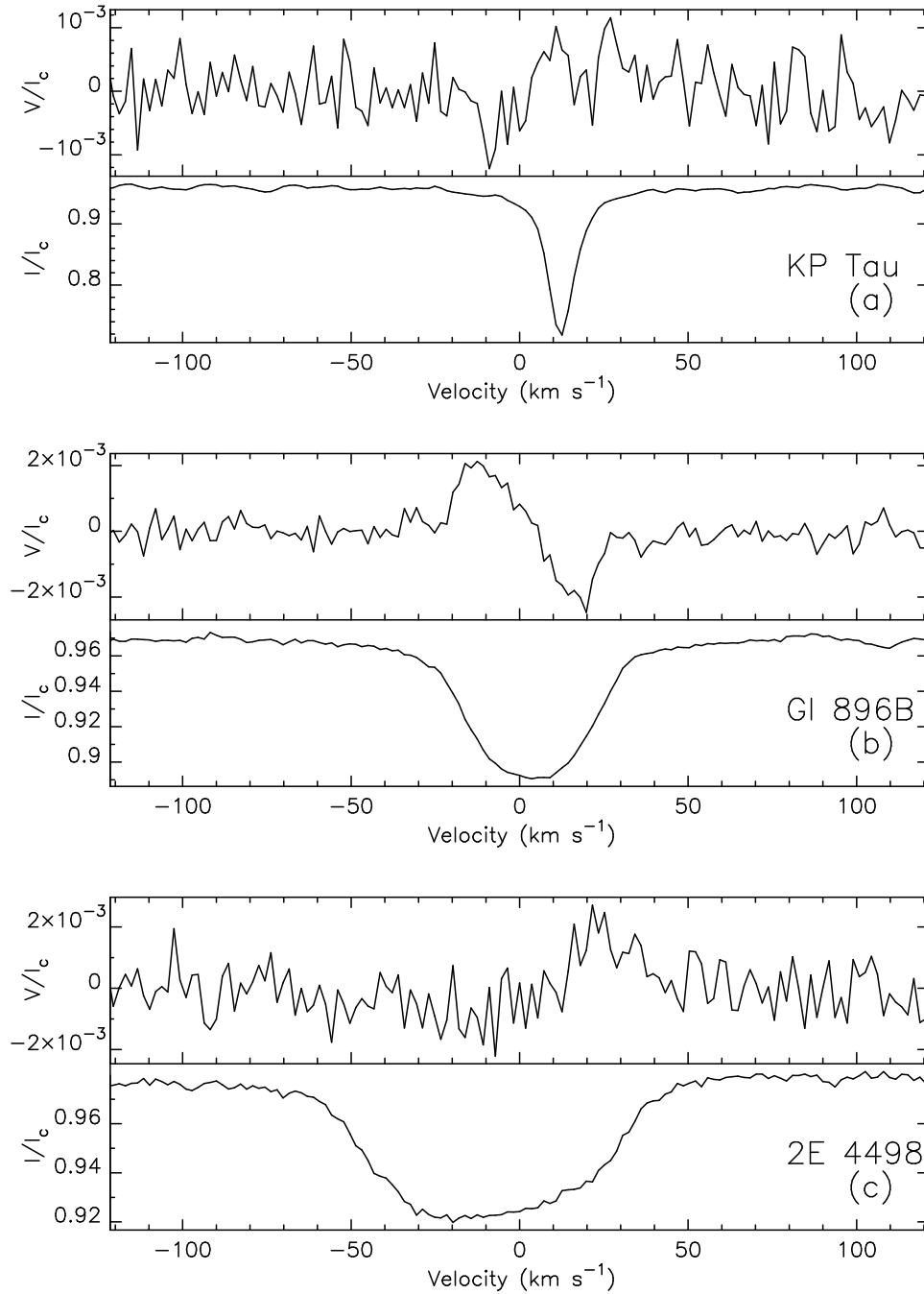


FIG. 1.— LSD Stokes V and I profiles of 3 M dwarfs: KP Tau (panel a), Gl 896B (b) and 2E 4498 (c). Strong circular polarization is seen in the three stars.

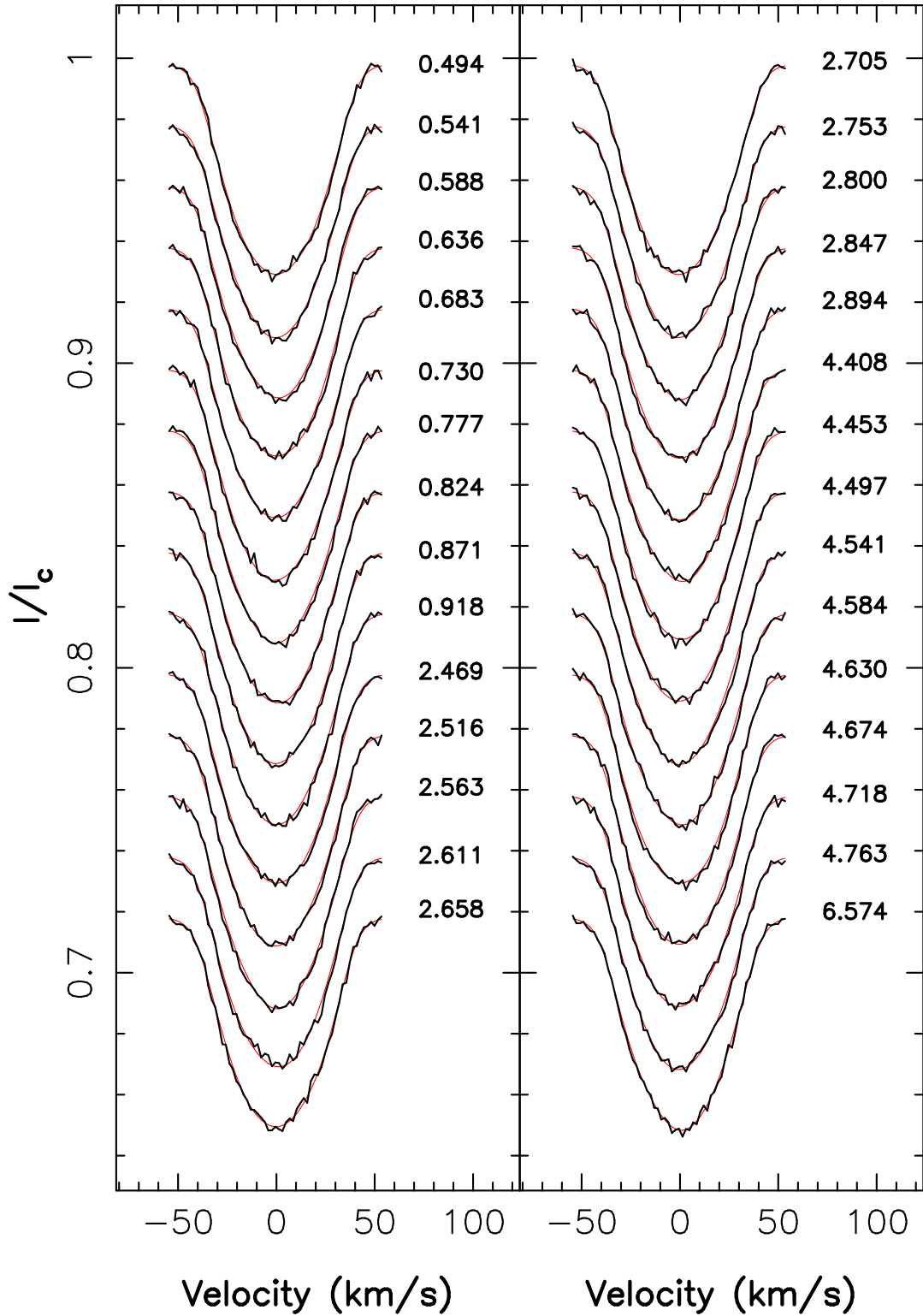


FIG. 2.— LSD Stokes I profiles of G 164-31 (black line) along with the maximum entropy fits (red line) to the data. The rotational phases are indicated to the right of each profile.

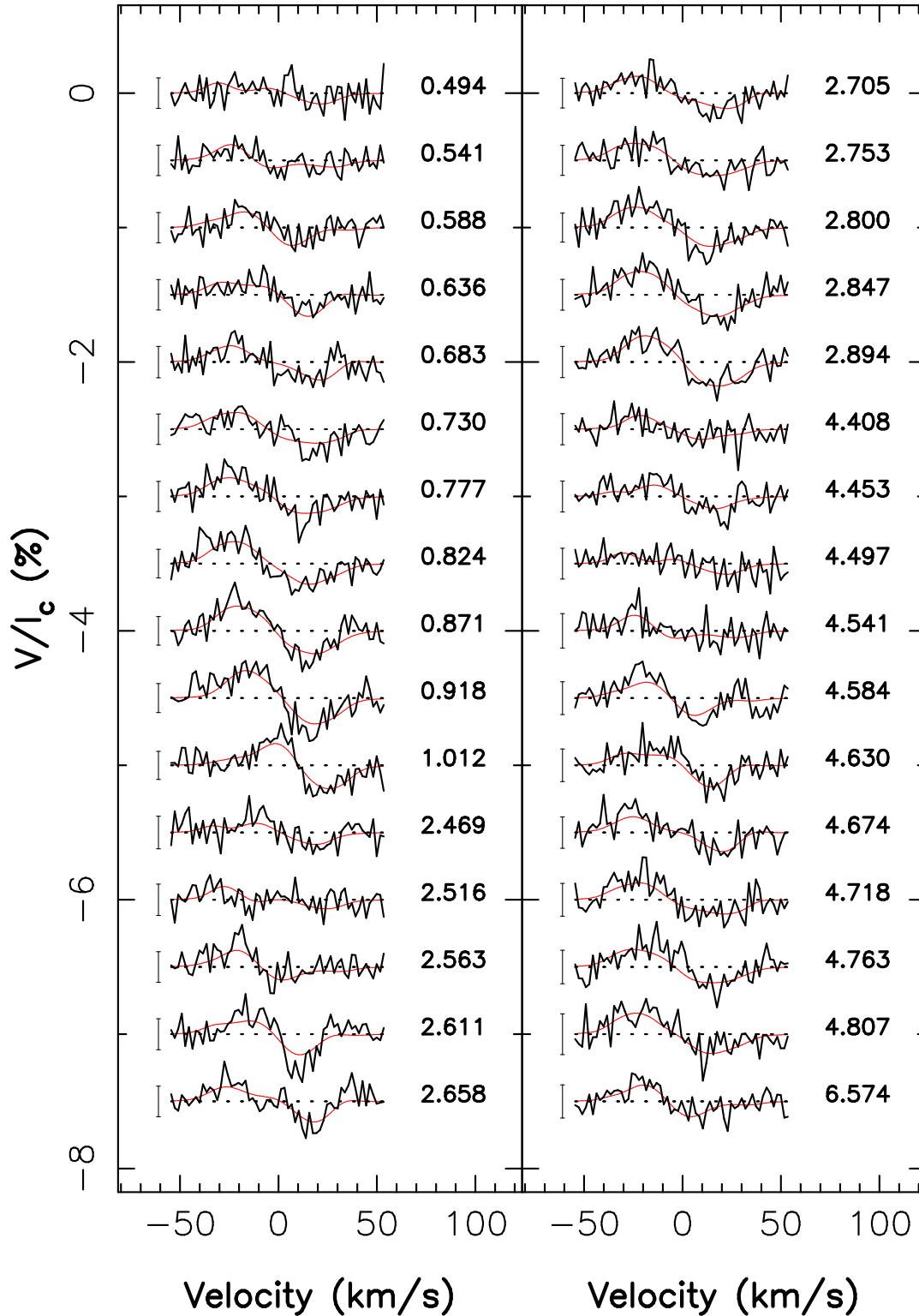


FIG. 3.— LSD Stokes V profiles of G 164-31 (black line) along with the maximum entropy fits (red line) to the data. The rotational phase (*right*) and the 3σ error bar (*left*) of each profile are shown accordingly.

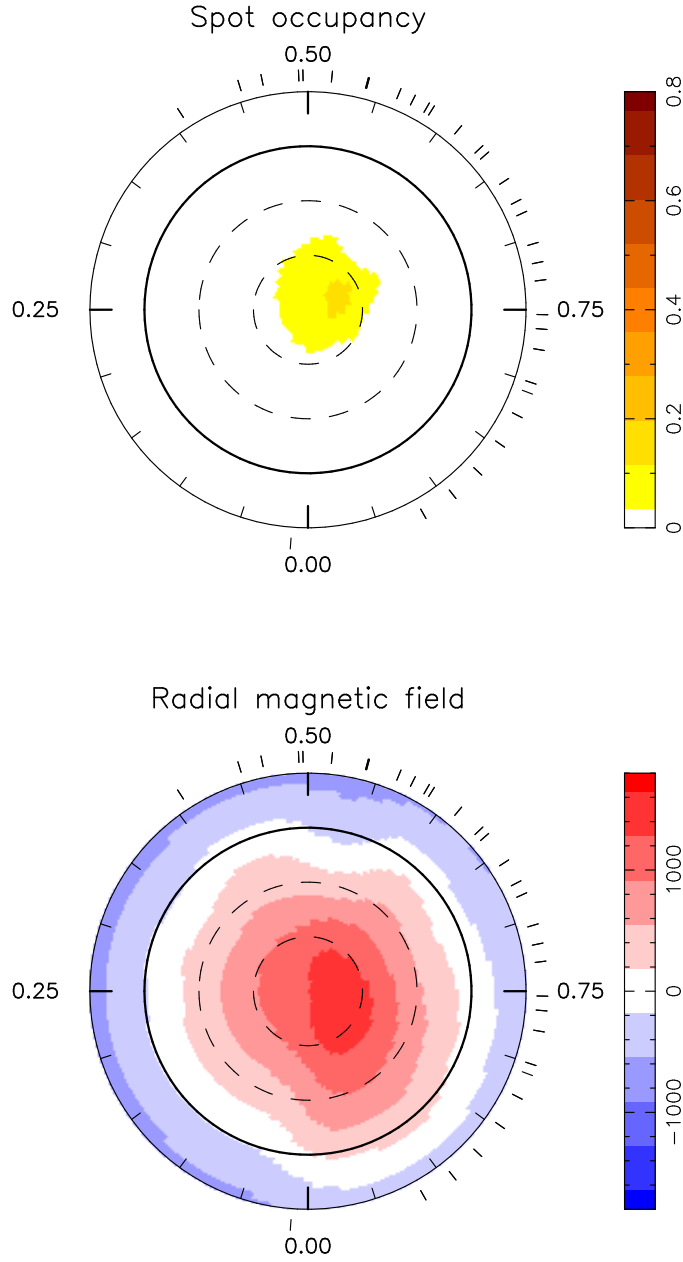


FIG. 4.— Magnetic field topologies of G 164-31, reconstructed from the series of LSD Stokes V profiles. The radial field (*bottom*) dominates in the dwarf (intensity scale in Gauss), the azimuthal and meridional component are negligible. The spottedness (*top*) at the stellar surface is also reconstructed, the color scale represents spot occupancy for the dwarf (1=complete spot coverage). The dwarf is shown in flattened polar projection extending down to latitudes of -30° . The equator is described as a bold circle. Radial ticks outside the plots indicate the phases at which the dwarf was observed, a half of the dwarf surface had properly been monitored.

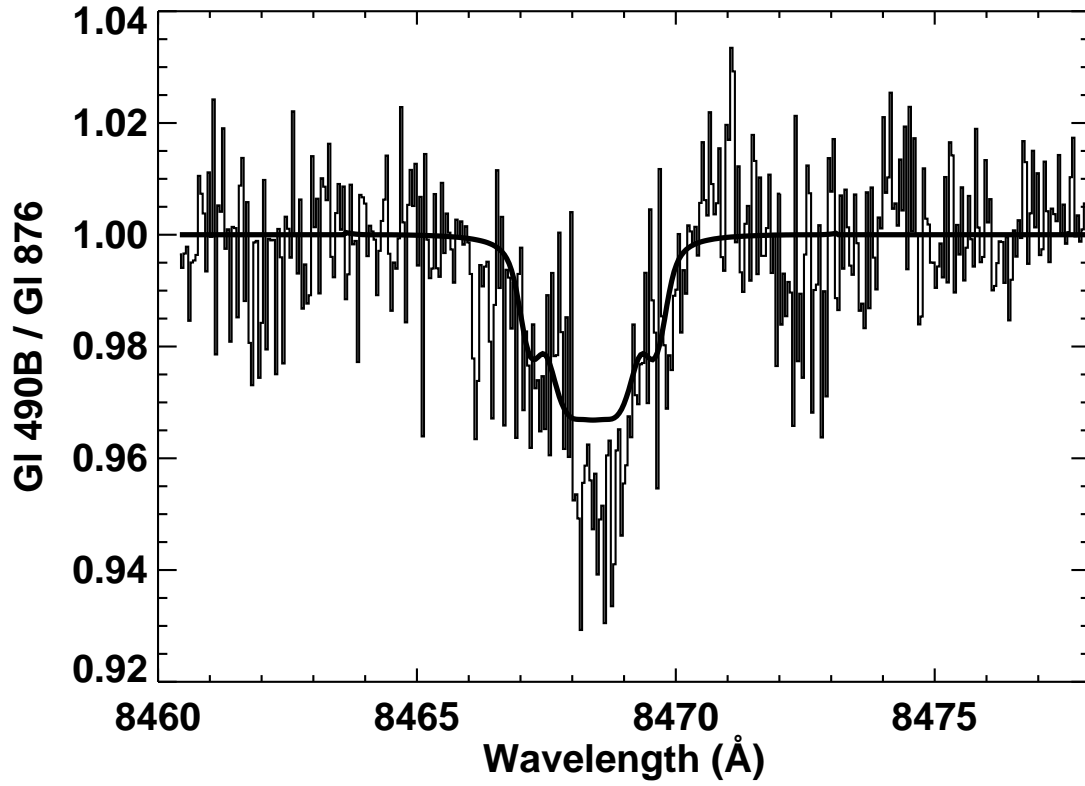


FIG. 5.— Best-fit modeling ratio of active to inactive profiles (thick line). The observed line profile ratio constructed by dividing the spectrum of G 164-31 (G1 490B) in the wavelength region around the magnetically sensitive Fe I line at 8468.4 Å by that of the inactive M4 dwarf G1 876 is shown (thin line).

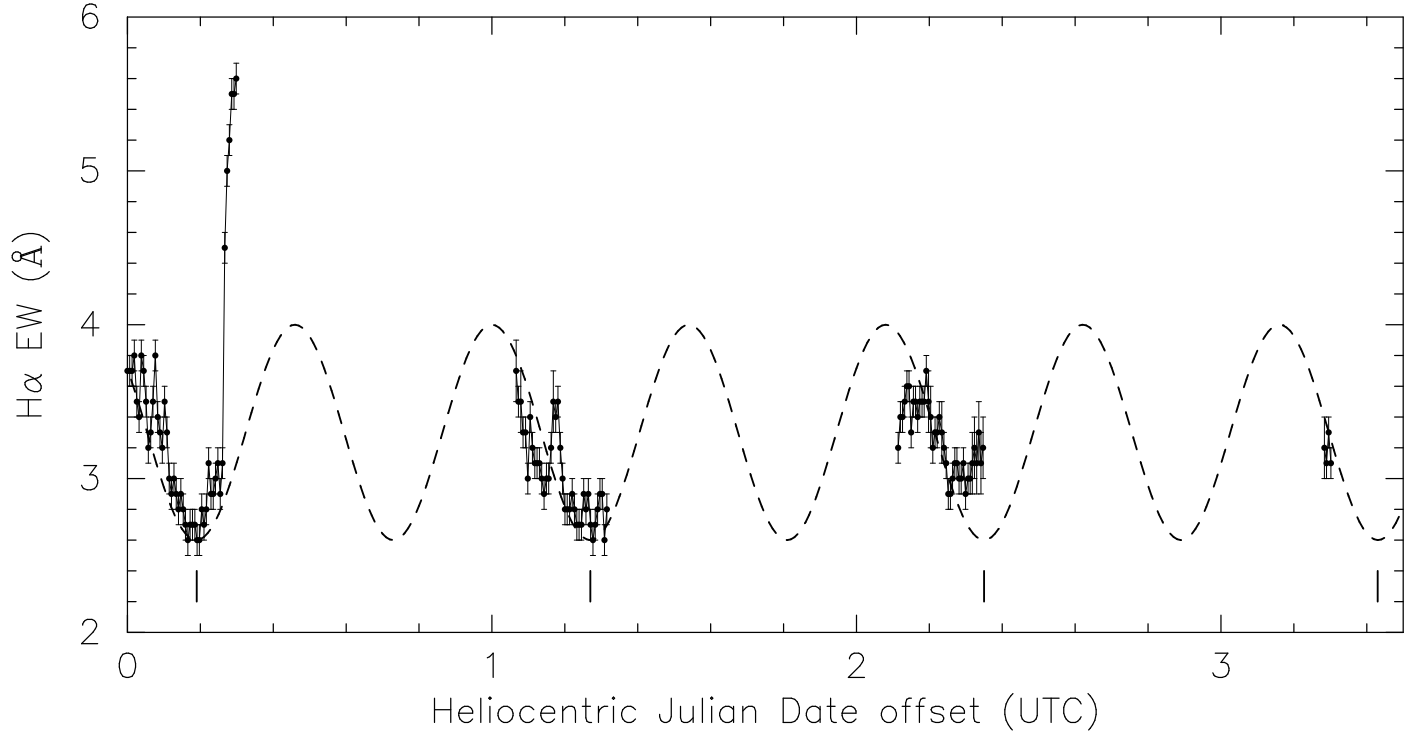


FIG. 6.— $H\alpha$ equivalent width light curve. The curve appears likely sinusoidal, a sinusoidal curve (dashed-line) is also shown for a comparison. The first vertical tick at 0.19 in the HJD offset (HJD-2454549.79717) position indicates the bottom of the light curve obtained in the first night. The remaining ticks are drawn with a distance of $2 \times P_{\text{rot}}$ between two consecutive ticks where the star is observable, where $P_{\text{rot}} = 0.54$ days is the rotational period determined from the Stokes V profile set (see § 3.2). The observed bottoms of the light curve likely repeat after $2P_{\text{rot}}$, suggesting that the $H\alpha$ emission is modulated by the stellar rotation. Flaring events were observed in the first (strong) and second night (moderate). The decay and enhancement of $H\alpha$ emission were also observed in the third night at around HJD offset=2.1 and 2.35, respectively. This is possibly due to a decrease (or an increase) of the number of active regions. Changes in the $H\alpha$ (also $H\beta$) line profile shape (e.g., smoothness) seen in our spectra support this possibility.